International Journal of Research in Engineering and Science (IJRES)
ISSN (Online): 2320-9364, ISSN (Print): 2320-9356
www.ijres.org Volume 14 Issue 4 ǁ April 2026 ǁ PP. 43-57

Aluminum Silicate Fiber Composite Mica Paper with Aramid and Plant Fibers for Electrical Insulation

Zhen-hui Wang,Li-ying Dong,Ying-jie Zhu
[*1]*Materials and Chemical Engineering, University of Shanghai for Science and Technology, Shanghai, China*
[2]*Shanghai Institute of Ceramics,Chinese Academy of Sciences, Shanghai, China*
Corresponding Author: Zhen-hui Wang

Abstract
Aluminum silicate fiber composite papers are valued for thermal insulation due to their high-temperature resistance and low cost. However, their application is limited by inadequate mechanical strength and insulation performance. In this work, a lightweight, high-strength aluminum silicate fiber composite mica paper (AFCSM) was fabricated by a conventional filtration molding and drying process. The influence of mica content (10, 20, 30, and 40 wt%) on the properties of the paper was systematically investigated. The physical properties, microstructure, mechanical strength, hydrophobicity, and electrical insulation of AFCSM were characterized. To isolate the role of silicone resin, composite papers without resin (AFCM) were also prepared for comparison. For samples prepared without silicone resin, tensile strength increased with mica content, reaching a maximum of 1.35 MPa at 40% mica. In contrast, resin-containing composites achieved optimal tensile performance of 1.75 MPa at 20% mica content. Dielectric strength improved significantly with increasing mica fraction; the highest value of 12.02 kV/mm was recorded for the resin-free paper with 40% mica. Surface treatment with a hydrophobic agent resulted in water contact angles exceeding 100°, indicating excellent water repellency. These results demonstrate that AFCSM paper can achieve a desirable balance of mechanical robustness, electrical insulation, and hydrophobicity. This cost-effective material shows promise for electrical insulation applications in power batteries and other demanding environments. This cost-effective, high-performance material shows a promising candidate for applications in power batteries and other environments demanding superior thermal and electrical insulation.

Keywords: *Aluminum silicate fiber, Mica, Silicone resin, Tensile strength, Hydrophobicity, Thermal and electrical insulation.*

Date of Submission: 26-03-2026 Date of Acceptance: 07-04-2026

I.INTRODUCTION

Lithium-ion batteries (LIBs) have become the dominant power source for electric vehicles and portable electronics owing to their high energy density, long cycle life, and low self-discharge rate [1]. However, the thermal safety of LIBs remains a critical concern, as they are susceptible to thermal runaway under abusive conditions [1]. Thermal runaway causes exothermic decomposition of electrode materials and electrolyte, generating heat, gas, and toxic fumes, which can lead to fire or explosion [2]. Therefore, understanding thermal runaway mechanisms and implementing effective thermal management strategies are essential for improving battery safety [1,2].

Thermal insulation of battery packs is a promising strategy to mitigate thermal runaway by placing insulation layers between cells [3]. Ideal interlayer materials should possess excellent thermal insulation, sufficient mechanical strength to withstand cell swelling and vibration, high dielectric strength to prevent electrical shorts, and hydrophobicity to resist moisture ingress [4]. Fiber materials can provide thermal insulation while maintaining good mechanical properties [5-7]. The development of advanced thermal insulation materials contributes to safer and more energy-efficient energy storage systems [8].

Fiber-based insulating papers have attracted considerable attention due to their low cost, light weight, flexibility, and ease of processing [9]. Traditional cellulose paper, however, suffers from limited thermal stability and poor mechanical properties at elevated temperatures [10]. To overcome these drawbacks, various inorganic and synthetic fibers have been incorporated into paper matrices [11]. Aluminum silicate fiber (AO) exhibits outstanding high-temperature resistance (melting point >1600 °C) and low thermal conductivity, making it suitable for thermal insulation applications [11]. Aramid fiber (AFS) offers excellent mechanical properties, thermal stability up to 400 °C, and intrinsic electrical insulation [12,13]. Cellulose fiber (CFS) can enhance mechanical integrity and improve slurry processability due to its porous structure [14]. Combining these fibers may yield a composite paper with balanced thermal, mechanical, and insulating properties.

In addition to fiber selection, the incorporation of functional fillers has been explored to further enhance performance. Mica, a layered aluminosilicate mineral, possesses high dielectric strength (up to 40 kV/mm), thermal stability, and chemical inertness [15]. When added to fiber networks, mica flakes can fill voids, create tortuous paths for charge carriers, and thereby increase the breakdown voltage of the composite [16]. Silicone resin (SI) is often used as a binder to improve interfacial bonding between fibers and fillers, as well as to impart flexibility and hydrophobicity [17]. However, the dispersion of mica and resin within the fiber matrix is challenging; surfactants such as fatty alcohol polyoxyethylene ether (AEO) are typically employed to achieve uniform distribution [18].

Several studies have reported on fiber-reinforced insulating composites. Tang et al. [19] modified cellulose paper with melamine-grafted nano-SiO_2 and observed enhanced mechanical strength and thermal stability, although nanoparticle aggregation remained an issue. Wei et al. [20] incorporated nano-boron nitride and nanocellulose into cellulose paper, achieving improved thermal conductivity and insulation, but the synthesis process was costly. Pan et al. [21] constructed a nacre-like aramid-mica nanopaper with excellent mechanical and insulating properties; however, its performance degraded under high humidity. These studies highlight the need for a cost-effective, scalable material that simultaneously offers robust mechanical strength, high dielectric strength, thermal stability, and hydrophobicity.

In this work, we designed a novel aluminum silicate fiber composite mica paper (AFCSM) by combining ASF, AF, CF, silicone resin, and mica flakes through a conventional papermaking process. The effects of mica content (10–40 wt%) on the microstructure, mechanical properties, dielectric strength, and hydrophobicity of the resulting composites were systematically investigated. For comparison, resin-free counterparts (AFCM) were also prepared to elucidate the role of silicone resin. The objective is to develop a lightweight, high-performance insulating paper suitable for battery thermal management, with a balanced set of properties meeting the demanding requirements of electric vehicle applications.

II.EXPERIMENTAL SECTION

2.1 Materials.

The following materials were used as received without further purification: aluminum silicate fiber (AO, length 2–4 mm, diameter 3–5 μm, Shanghai Wendao Industrial Co., Ltd., China); aramid fiber (AFS, length 4–6 mm, diameter 10–12 μm, DuPont™ Kevlar®, USA); cellulose fiber (CFS, bleached softwood kraft pulp, average length 2.5 mm, Yongfeng Paper Co., Ltd., China); mica sheets (MC, particle size 20–40 μm, Chutian Mica Co., Ltd., China); silicone resin (SI, methyl phenyl silicone resin, solid content 50%, viscosity 20–40 mPa·s, Shanghai Resin Factory Co., Ltd., China); fatty alcohol polyoxyethylene ether (AEO, analytical grade, Sinopharm Chemical Reagent Co., Ltd., China); hydrophobic sizing agent (TF-3002R, Transfar Chemicals, China); and deionized water (laboratory-made, resistivity >18 MΩ·cm).

2.2 Preparation of Composite Mica Paper

The composite papers were fabricated using a conventional handsheet former (PTI, Austria) following a modified filtration molding method. The target basis weight for all samples was 600 g/m². The dry mass ratio of ASF:AF:CF was fixed at 80:10:10 based on preliminary optimization studies. SI was added at 10 wt% of the total fiber mass, while MC were incorporated at 10, 20, 30, and 40 wt% relative to the total fiber mass.

For a typical preparation (Figure 1a), the fibers (AO, AFS, CFS) were first dispersed in deionized water containing 0.3 wt% AEO as a dispersant. The mixture was stirred at 800 rpm for 10 min to ensure homogeneous fiber suspension. For resin-containing samples, SI was added dropwise under continuous stirring. MC were then introduced according to the desired content, and the slurry was stirred for an additional 10 min. The total mass of the slurry was adjusted with deionized water to achieve a fiber concentration of 0.5 wt%.

The well-dispersed slurry was poured into the handsheet former (forming area 0.0314 m²) and allowed to drain by gravity. The wet mat was then pressed at 0.5 MPa for 5 min to remove excess water, followed by drying in a convection oven at 105 °C for 10 min. The obtained composite papers were designated as AFCSM-x, where x represents the MC content (10, 20, 30, 40). For comparison, resin-free composite papers (AFCM-x) were prepared following the same procedure but without the addition of SI. Figure 1b–d shows photographs of the fiber slurries, wet sheets, and final dried papers, respectively.

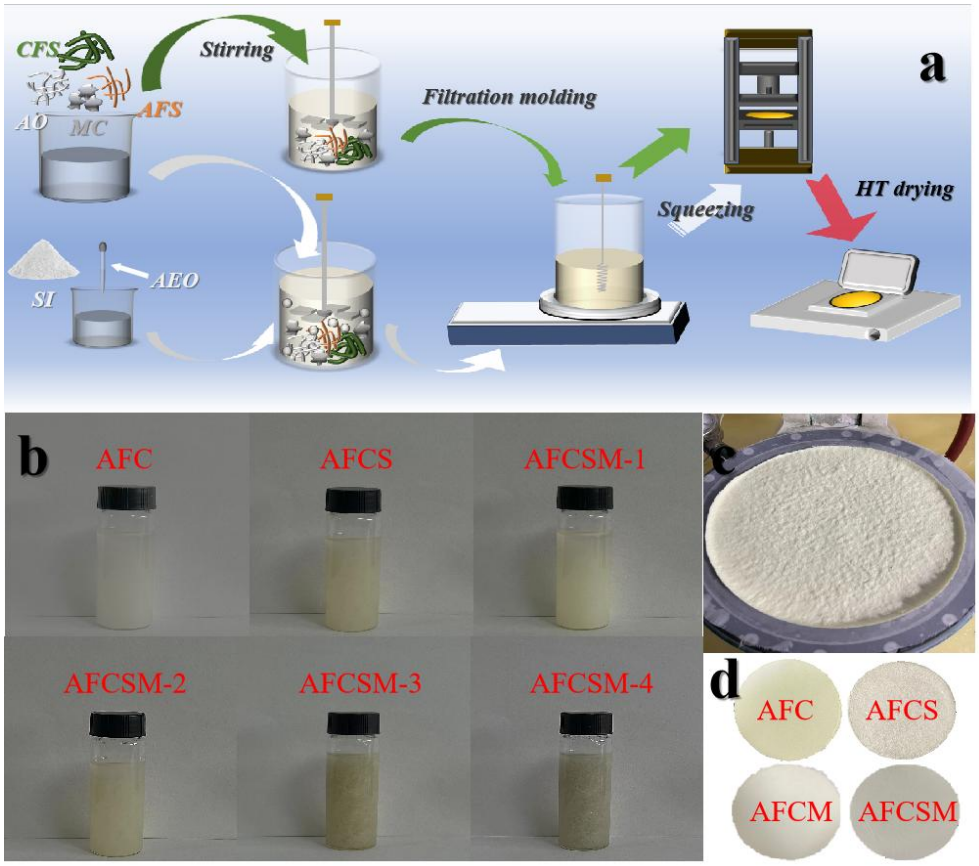

Figure 1. (a)Schematic diagram of AFCSM/AFCM preparation. (b) Slurry state of AFC/AFCS/AFCSM 1-4. (c) Paper sheet preliminary forming diagram. (d) Composite fiber paper (AFC/AFCS/AFCM/AFCSM) forming pictures.

2.3 Physical Properties

The grammage (basis weight) of each paper sample was determined by weighing five 100 mm × 100 mm specimens and calculating the average mass per unit area (g/m²). Thickness was measured using a digital micrometer (Mitutoyo, Japan) with a resolution of 1 μm; ten random positions on each sample were measured, and the average value was reported. Density (ρ, g/cm³) was calculated as $\rho = W / t$, where W is the grammage (g/m²) and t is the thickness (μm) after unit conversion. Bulk (B, cm³/g), the reciprocal of density, was calculated as $B = 1/\rho$.

2.4 Scanning Electron Microscopy (SEM)

The surface morphology of the samples was examined using field-emission scanning electron microscopy (FE-SEM, Hitachi S-4800, Japan) operated at an accelerating voltage of 15 kV. Prior to observation, samples were sputter-coated with a thin layer of gold to improve conductivity.

2.5 Tensile Strength Test

Tensile strength was measured using a universal tensile tester (AT-L-1, Hangzhou Qingtong Boke Co., Ltd., China) at room temperature (25 ± 2 °C) and 50 ± 5% relative humidity. Specimens were cut into rectangular strips of 50 mm × 15 mm. The gauge length was set to 30 mm, and the crosshead speed was 5 mm/min. Ten replicates were tested for each sample type, and the mean value was calculated after excluding outliers using the Grubbs' test ($\alpha = 0.05$).

2.6 Dielectric Strength Test

Dielectric strength was evaluated using a breakdown voltage tester (CS2674A, Nanjing Changsheng Instrument Co., Ltd., China) according to ASTM D149-09. Circular specimens with a diameter of 75 mm were placed between two cylindrical brass electrodes (25 mm diameter) immersed in silicone oil to prevent surface flashover. An alternating voltage (50 Hz) was applied and increased at a constant rate of 0.2 kV/s until dielectric breakdown occurred. The breakdown voltage (V, kV) and the thickness at the breakdown site (d, mm) were

recorded. Dielectric strength (E, kV/mm) was calculated as E = V/d. Five measurements were performed for each sample, and the average value was reported.

2.7 Hydrophobicity Test

Static water contact angles were measured using a contact angle goniometer (DSA100, Krüss, Germany) at 25 ± 1 °C. The composite papers were first treated with TF-3002R hydrophobic sizing agent by spray coating, followed by drying at 105 °C for 6 h. A 5 μL deionized water droplet was dispensed onto the sample surface, and the contact angle was recorded within 10 s of droplet deposition. Five different positions on each sample were measured, and the average value was calculated.

2.8 Thermal Analysis

Differential scanning calorimetry (DSC) was performed using a thermal analyzer (DSC 214 Polyma, Netzsch, Germany) to evaluate the thermal stability of the composite papers. Samples (5–10 mg) were placed in aluminum pans and heated from 30 to 600 °C at a rate of 10 °C/min under a nitrogen atmosphere (flow rate 50 mL/min). An empty aluminum pan was used as a reference.

III.RESULTS AND DISCUSSION

A high proportion of aluminum silicate fiber (AO) is essential for achieving excellent high-temperature performance and structural stability in fiber-based insulating materials. To establish the optimal fiber composition for the composite paper, we first investigated the thermal insulation performance of binary fiber systems with varying AO:CFS and AO:AFS ratios.

Figures 2a and 2b show the surface temperature evolution of the fiber composites under alcohol lamp heating for 600 s. In both systems, increasing the content of cellulose fiber (CFS) or aramid fiber (AFS) reduced the thermal insulation performance. During the first 10 min of heating, the composite with the highest ASF content (80%) exhibited the lowest surface temperature rise, confirming the dominant role of ASF in thermal protection.

After 600 s of heating, the composite with 20% CF and 80% ASF reached a final surface temperature of 411 °C, corresponding to a temperature difference (ΔT) of 139 °C relative to the hot plate temperature (550 °C). In comparison, the composite with 20% AFS and 80% ASF reached 393 °C with a ΔT of 157 °C (Table 1). These results indicate that while both CFS and AFS reduce thermal insulation when substituted for ASF, AF has a less pronounced effect than CF at equivalent loadings.

Table 1: Thickness, final temperature and temperature difference of AO and CFS/AFS composites with different contents after heating for 600s

fiber ratio(%)	Fiber Composition	Thickness（mm）	Temperature (600s)	Temperature difference
CK	100% AO	——	550°C	
20CFS	20% CFS+80% AO	1.193	411°C	139°C
30CFS	30% CFS+70% AO	1.223	422°C	128°C
40CFS	40% CFS+60% AO	1.276	463°C	87°C
50CFS	50% CFS+50% AO	1.198	500°C	50°C
20AFS	20% AFS+80% AO	0.615	393°C	157°C
30AFS	30% AFS+70% AO	0.763	442°C	108°C
40AFS	40% AFS+60% AO	0.686	448°C	102°C
50AFS	50% AFS+50% AO	0.807	461°C	89°C

Thermal insulation alone, however, is insufficient for practical applications; mechanical integrity must also be considered. Figures 2c and 2d present the tensile strength of the same fiber composites. In contrast to the insulation behavior, tensile strength increased with higher CFS or AFS content. Both CFS and AFS act as structural reinforcements within the AO network: CFS enhances fiber-fiber entanglement through its flexible morphology, while AFS provides high-modulus reinforcement that resists crack propagation.

These opposing trends—decreasing insulation but increasing mechanical strength with higher CFS/AFS content—necessitate a balanced fiber formulation. Excessive replacement of AO with CFS or AFS should be avoided, as it compromises thermal insulation and can increase brittleness, particularly at high CFS loadings. Small additions of CFS or AFS (≈10%) can improve mechanical properties while preserving the high-temperature resistance conferred by the ASF matrix.

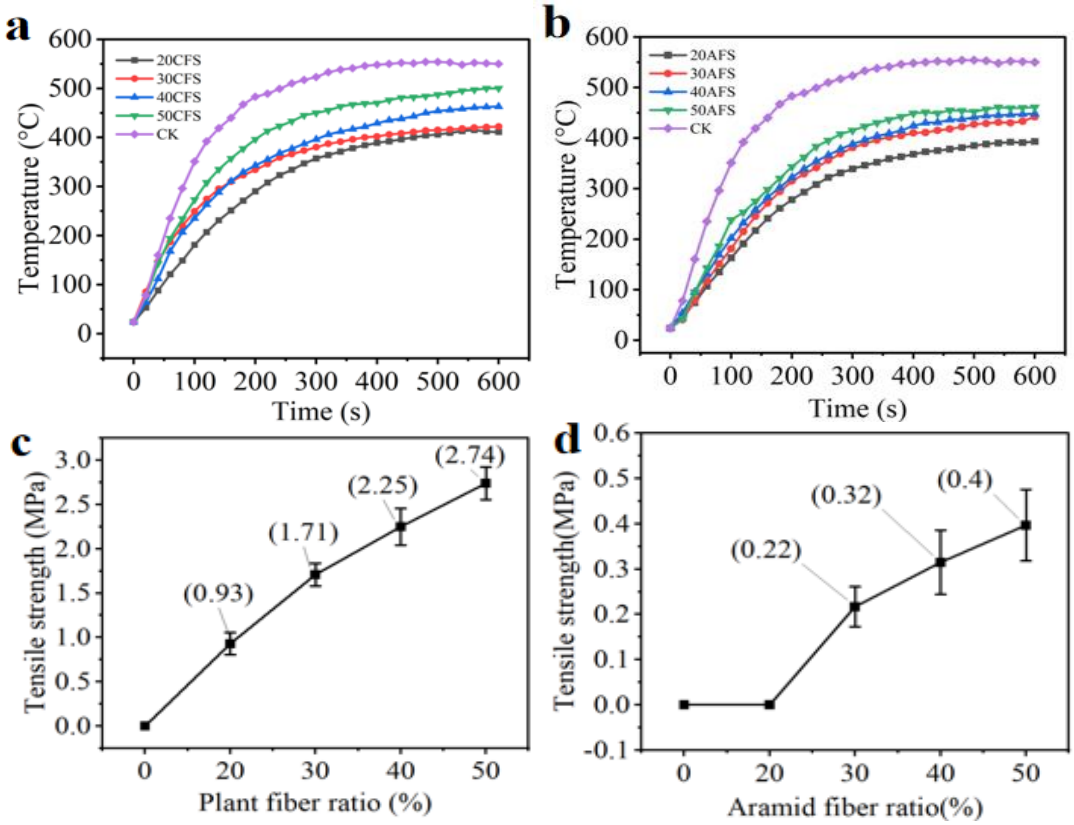

Figure 4:(a, b) Surface temperature evolution of fiber composites with different AO:CFS and AO:AF ratios under alcohol lamp heating for 600 s. (c, d) Tensile strength of fiber composites with varying AO:CFS and AO:AFS ratios.

3.1 Effect of Silicone Resin on Composite Properties

Silicone resin (SI) can enhance the mechanical properties of composite paper at high temperatures (400 °C) [15]. To evaluate its role in the present system, we prepared aluminum silicate fiber composites (AFC, i.e., AFCSM without mica) with varying SI content and characterized their tensile strength and dielectric strength.

Figure 3a shows the effect of SI content on the tensile strength of AFC at room temperature. The tensile strength increased with SI addition, reaching 1.18 MPa at 10 wt% SI. This improvement is attributed to the resin's ability to penetrate the fiber network, fill interfacial voids, and form physical bonds between fibers, thereby enhancing stress transfer [15]. After heat treatment at 400 °C for 30 min, the tensile strength of all samples increased (Figure 3b). For the composite with 10 wt% SI, the tensile strength reached 2.76 MPa, representing a 134% increase compared to its room-temperature value. This enhancement likely results from further crosslinking of the silicone resin at high temperature, which strengthens the fiber-resin interfacial bonding [25]. Notably, the addition of SI did not compromise the electrical insulation properties. The dielectric strength of AFC remained relatively constant at approximately 3 kV/mm across all SI contents tested (Figure 3c). This indicates that silicone resin can be used to improve mechanical robustness without degrading the insulating performance of the fiber composite [15].

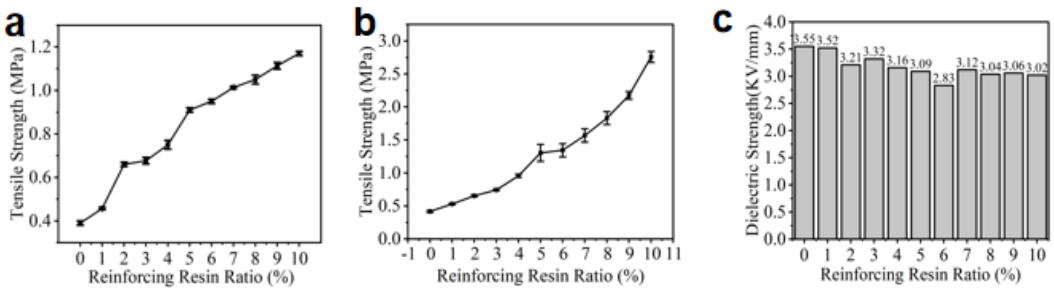

Figure 2(a) Effect of silicone resin addition on tensile strength of composite fiber paper (AFC). (b)AFC tensile strength of composite fiber paper with different content of silicone resin after standing for 30min at 400°C. (c)Effect of silicone resin addition on dielectric strength of composite fiber paper (AFC).

3.2 Microstructural Characterization

Figure 4a shows the morphology of pure aluminum silicate fiber (AO). The AO appears as long, smooth fibers with uniform diameters and a random orientation [22]. Figure 4b shows the AO/CFS composite. Cellulose fibers (CFS) exhibit a relatively thick and rough morphology with a porous network structure. In some regions, the CFS adhere to the AO surfaces. Physical adhesion between the CFS microfibrils and AO contributes to the mechanical strength of the paper [13].

Figure 4c shows the AO/AFS composite. Aramid fibers (AFS) are cylindrical and thick, physically interconnecting with the AO network. However, in the absence of silicone resin (SI), local fiber slippage may occur. The AO form a solid with smooth, cylindrical AFS dispersed among them, while flexible CF fill the interstitial gaps. Without SI, sub-micron voids are visible at the fiber interfaces (Figure 4d). When SI is added (Figure 4e), a uniform coating covers the fibers, filling gaps and creating a more compact structure. It is hypothesized that Si-O-C covalent bonds form at the AO/AF interface, while hydrogen bonding is strengthened at the AO/CFS interface [15,17].

Figure 4f shows the morphology of mica sheets (MC). The MC exhibit a flaky structure with a smooth surface and strong inherent adhesion [17,18,28]. Figure 4g presents a schematic diagram of the internal structure of the composite paper, illustrating the overlapping fiber network with MC coated on the fiber surfaces. MC possess unique chemical, electrical, mechanical, and thermal properties that make them suitable for demanding industrial applications [26].

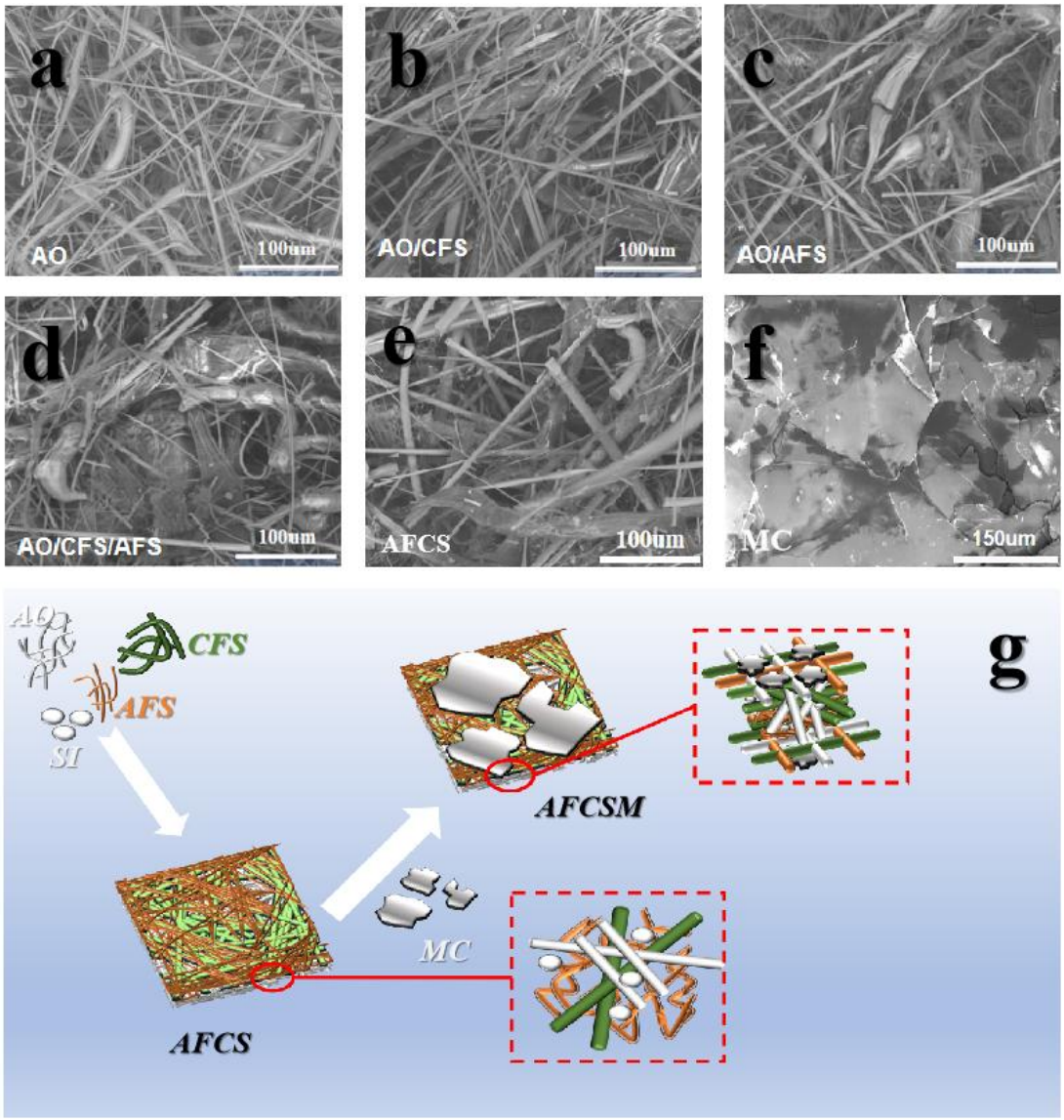

Figure 3 Microstructure of (a) AO, (b) AO/CFS, (c) AO/AFS, (d) AFC, (e) AFCS, (d) MC. (g) Internal lap diagram of composite fiber.

3.2 Basic Physical Properties of Resin-Free Composite Papers (AFCM)

Figure 5a shows the grammage of AFCM papers as a function of mica content. The grammage increased progressively with higher mica loadings, indicating effective retention of mica flakes during the sheet forming process. Thickness also increased with mica content (Figure 5b), which is attributed to the high aspect ratio and flaky morphology of mica flakes occupying greater three-dimensional space within the fiber network [17]. Density and bulk, calculated from grammage and thickness, are presented in Figures 5c and 5d. As mica content increased, density increased while bulk decreased, reflecting a more compact structure resulting from mica filling inter-fiber voids [28].

Figure 4e shows an SEM image of AFCM-20, revealing a dense network of interwoven fibers with uniformly distributed mica flakes [18]. The photograph of AFCM-30 (Figure 4f) confirms a flat, uniform surface.

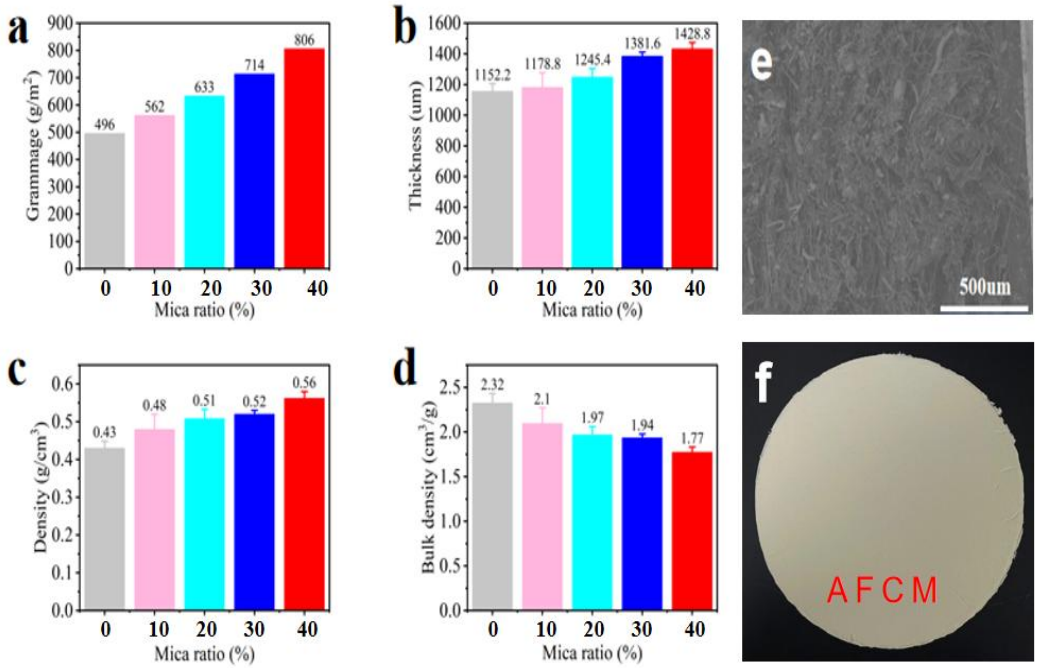

Figure 4.Basic Properties of AFCM: (a) grammage, (b) thickness, (c) density, (d) bulk density. (e) Microstructure of AFCM. (f) Electronic photo of AFCM.

3.3 Basic properties of composite papers with added silicone resin (AFCSM)

Figure 6a presents the grammage of AFCSM papers. The trend parallels that of AFCM, confirming consistent mica retention regardless of silicone resin addition. However, AFCSM papers exhibited markedly higher thickness—approximately 30% greater than AFCM at equivalent mica loadings (Figure 6b). This increase arises from the effect of silicone resin on fiber and mica dispersion. The low surface tension of silicone resin facilitates penetration into the fiber network, filling voids and coating fiber and mica surfaces, thereby increasing the overall volume of the composite [15]. The surfactant AEO promotes uniform resin dispersion, reducing agglomeration and contributing to a more open structure [18].

Consequently, AFCSM papers showed slightly lower density and higher bulk compared to AFCM (Figures 6c and 6d), consistent with the increased thickness. Figure 4g presents a schematic diagram of the internal structure, illustrating the "fiber-mica-resin" multilayer configuration. The photograph of AFCSM-30 (Figure 4f) confirms good sheet formation.

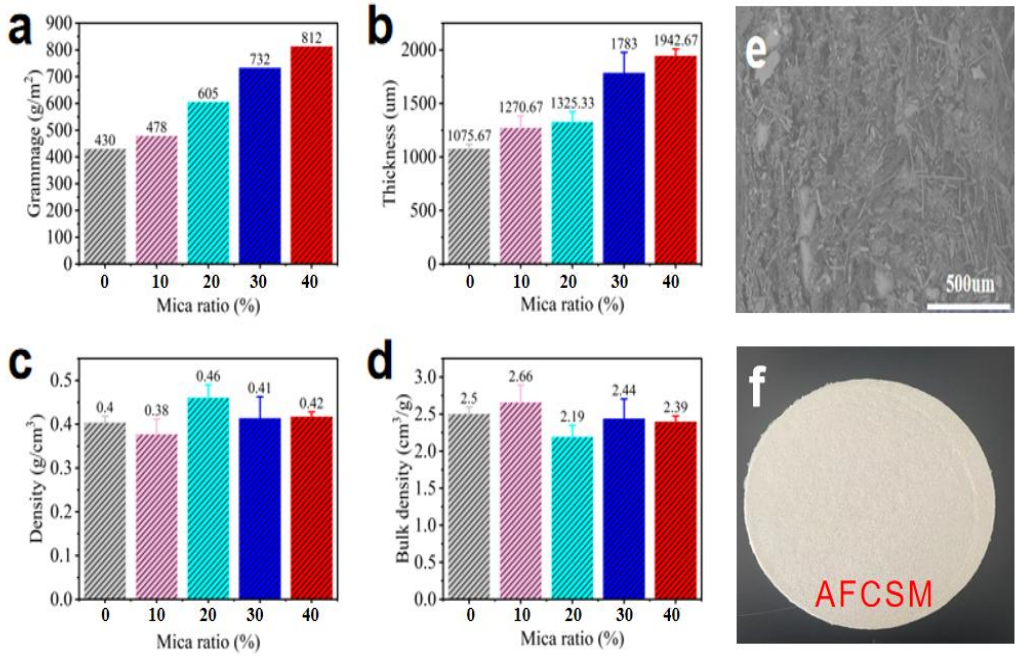

Figure 5. Basic Properties of AFCSM:(a) grammage, (b) thickness, (c) density, (d) bulk density. (e) Microstructure of AFCSM. (f) Electronic photo of AFCSM.

3.4 Analysis of Mechanical Properties

3.4.1 Tensile strength of AFCM

Figure 7a shows the tensile strength of AFCM composites as a function of mica content. The base composite (0% mica) exhibited a tensile strength of 1.1 MPa. With the addition of 10% mica, the strength increased to 1.35 MPa, indicating that mica flakes contribute to mechanical reinforcement at low loadings [19]. However, further increases in mica content led to a progressive decline in tensile strength, suggesting an optimal mica loading around 10% for the resin-free system.

This non-monotonic behavior can be explained by examining the microstructure. At 10% mica content, SEM images reveal that mica flakes are uniformly dispersed within the fiber network (Figure 7b). The lamellar morphology of mica enhances mechanical interlocking with fibers, creating an interpenetrating structure that hinders crack propagation [18]. Additionally, mica flakes fill micron-scale voids between fibers (Figure 7c), reducing stress concentration sites and increasing material density [28].

At higher mica contents (≥20%), however, the failure mode shifts from fiber-dominant to mica-dominant. Excessive mica introduces brittleness, as crack propagation occurs preferentially through the brittle mica lamellae rather than through the fiber network [18]. At 30% mica loading, SEM images show the formation of a continuous mica network with a surface coverage exceeding 75% (Figure 7d). This continuous mica phase disrupts the physical entanglement and hydrogen bonding between fibers [13]. At 40% mica, localized agglomeration and interfacial debonding become evident (Figure 7e), creating micron-scale defects that further compromise mechanical integrity [17].

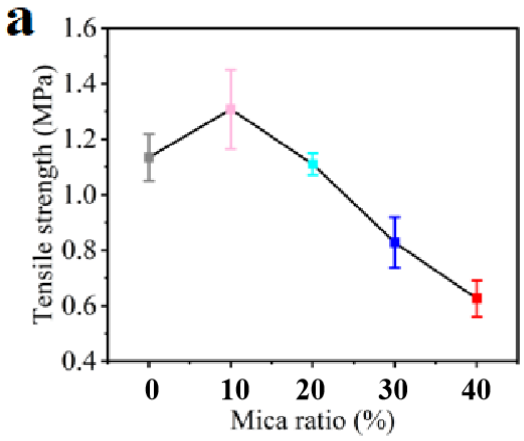

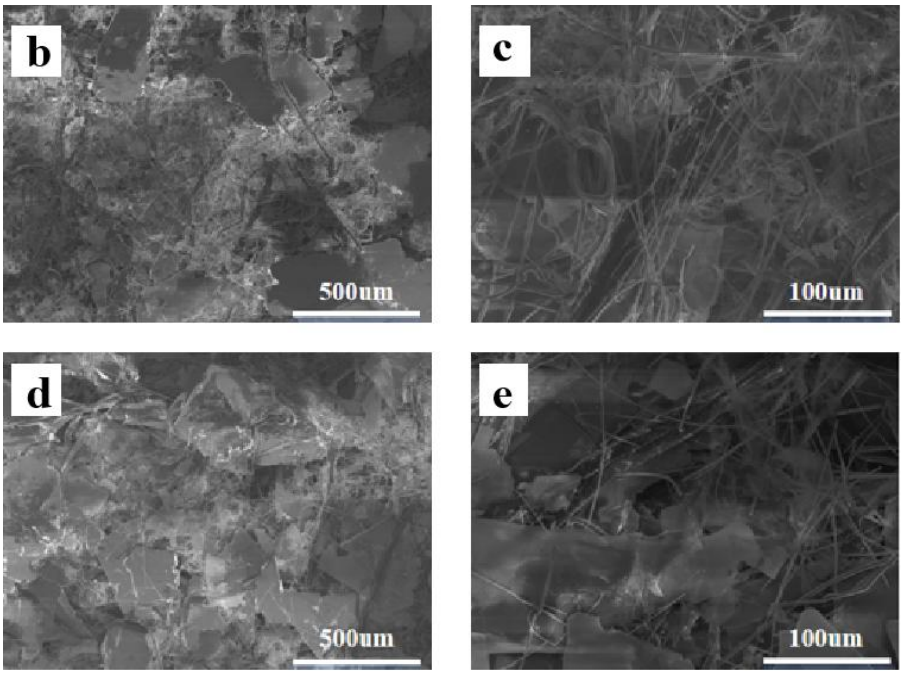

Figure 6 (a) Schematic diagram of tensile strength of AFCM changing with mica content. Microstructure of (b) AFCM-1, (c) AFCM-2, (d)AFCM-3, (e)AFCM-4

3.4.2 Tensile strength of AFCSM

Figure 8a presents the tensile strength of AFCSM composites with varying mica content. The addition of silicone resin significantly enhanced the mechanical performance compared to the resin-free system. The base AFCSM composite (0% mica) showed a tensile strength of approximately 1.6 MPa, substantially higher than the 1.1 MPa of AFCM. With increasing mica content, the tensile strength initially increased, reaching a maximum of 1.75 MPa at 20% mica, before declining at higher loadings [15].

Figure 8b directly compares the tensile strength of AFCM and AFCSM across all mica contents. The improvement conferred by silicone resin is evident at every mica loading, with the most pronounced enhancement occurring at 20% mica [15].

The enhanced performance of AFCSM composites is attributed to several factors. The surfactant AEO promotes uniform dispersion of mica flakes, minimizing agglomeration and reducing stress concentration sites [18]. Silicone resin effectively wets the mica surfaces and fiber networks, forming strong interfacial bonds [15]. At low to moderate mica contents (10–20%), SEM images reveal a dense, well-integrated structure with mica flakes uniformly embedded in the fiber-resin matrix (Figures 8c and 8d). The resin fills inter-fiber and fiber-mica gaps, creating a cohesive network that efficiently transfers stress [19].

At mica contents exceeding 20%, however, a similar transition to brittle behavior occurs. The formation of a continuous mica network becomes dominant, and the toughening effect of the fiber-resin matrix is overshadowed by the intrinsic brittleness of mica [18]. SEM images of AFCSM-30 and AFCSM-40 (Figures 8e and 8f) show evidence of mica agglomeration and localized micro-cracks, consistent with the observed decline in tensile strength [17].

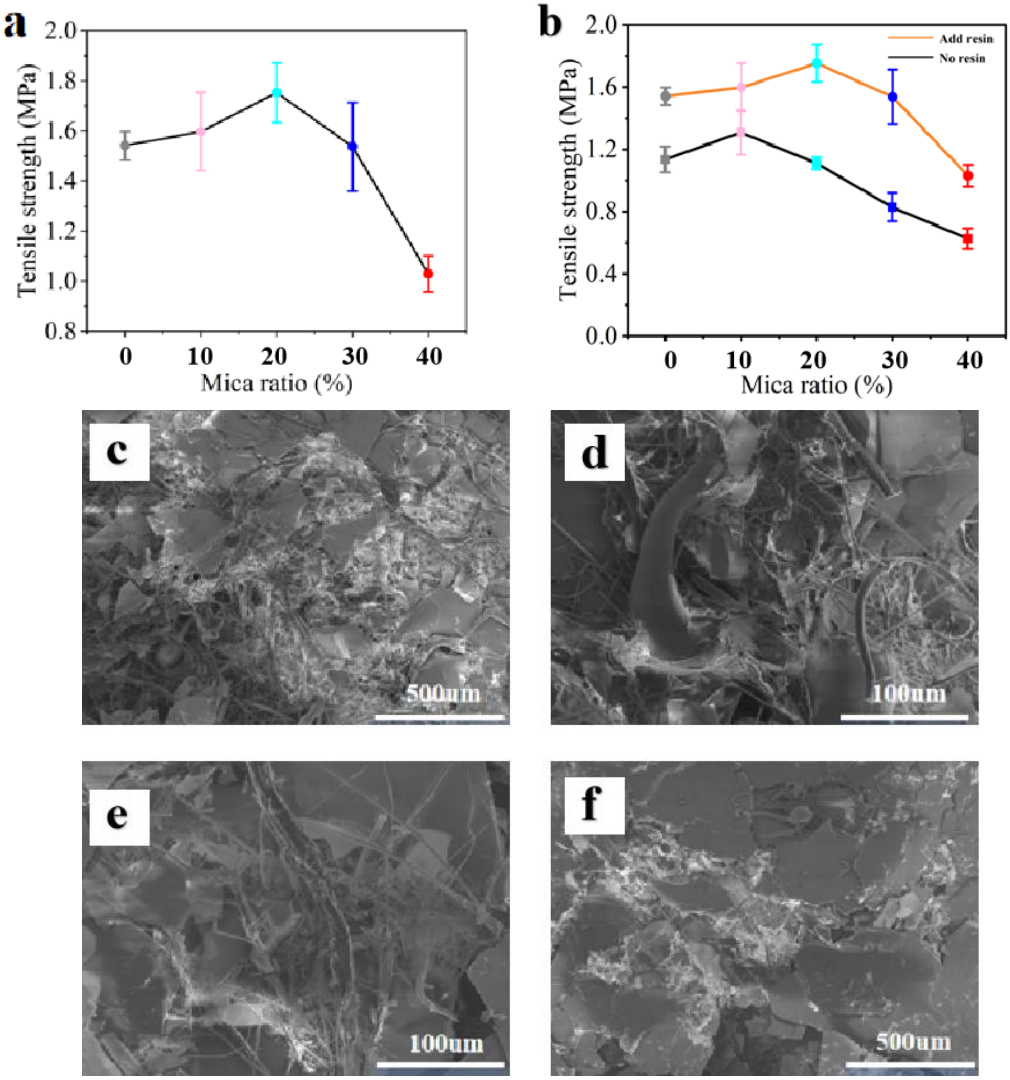

Figure 7. (a) Schematic diagram of tensile strength of AFCSM changing with mica content. (b) Comparison of tensile strength between AFCM and AFCSM. Microstructure of (c) AFCSM-1, (d) AFCSM-2, (e)AFCSM-3, (f) AFCSM-4

3.5. Analysis of insulation performance

3.5.1 Dielectric strength of AFCM

Figure 9a shows the dielectric strength of AFCM composites as a function of mica content. A clear positive correlation was observed: dielectric strength increased steadily with increasing mica loading, from 3.37 kV/mm at 0% mica to 10.14 kV/mm at 40% mica. This enhancement is attributed to the unique "brick-and-mortar" architecture of the composites (Figure 10) [16]. Mica flakes, with their lamellar morphology and high intrinsic dielectric strength, act as insulating "bricks" that fill voids between fibers and create tortuous pathways for charge carriers [19]. As mica content increases, the flakes progressively form a more continuous insulating network, effectively blocking conductive pathways and increasing the breakdown voltage [28,29].

At lower mica contents (10–20%), mica flakes are dispersed as discrete islands within the fiber network. While they contribute to insulation by filling local voids, continuous conductive pathways may still exist through fiber-fiber contacts. At higher mica contents (30–40%), the flakes begin to overlap and form a more interconnected network, significantly reducing the probability of direct fiber-fiber contact and thereby enhancing dielectric strength [16].

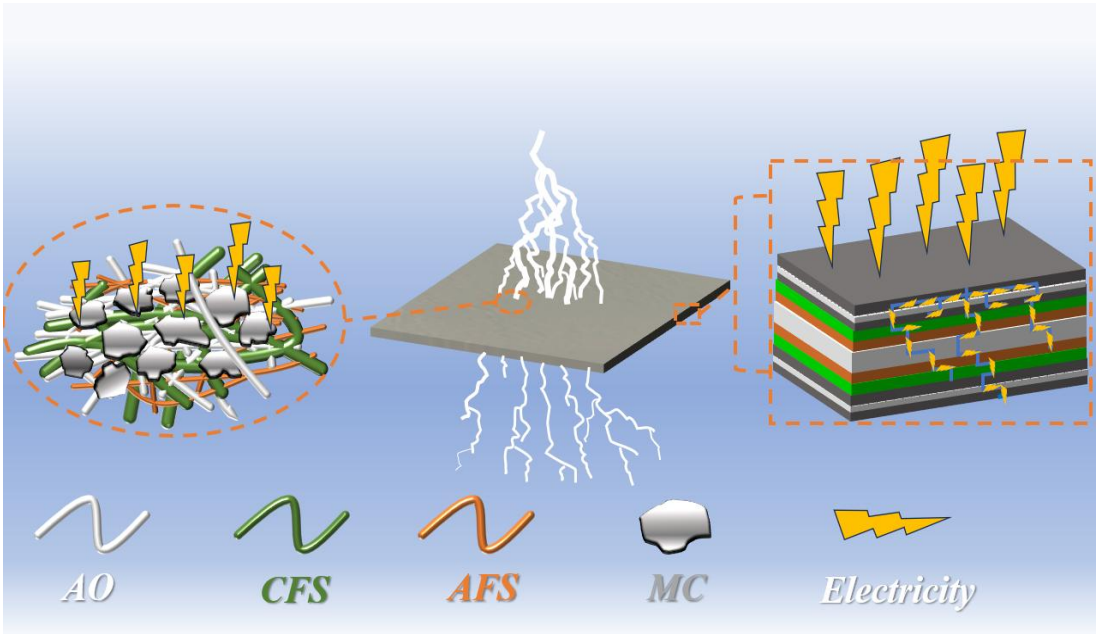

Figure 8.Schematic models of electric current transfer in AFCSM composite papers.

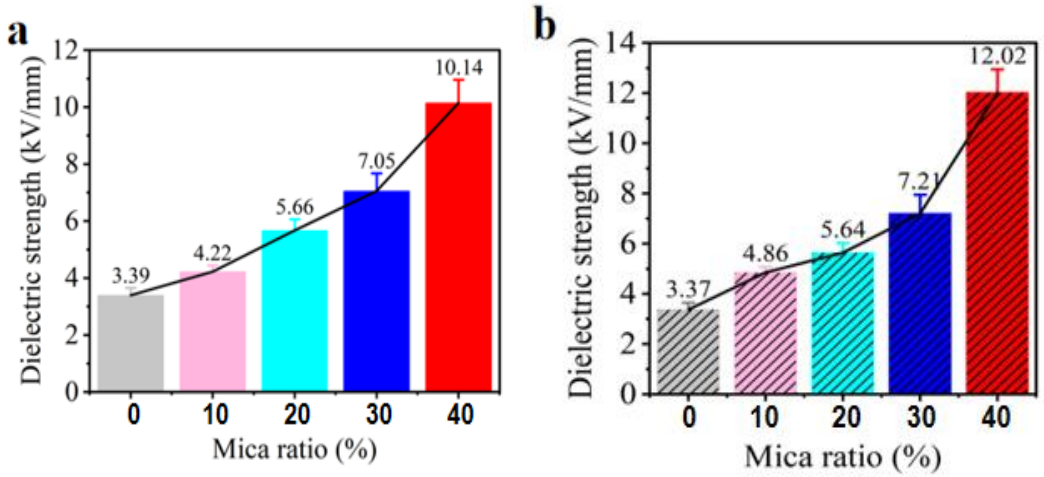

Figure 9. Dielectric strength performance of composite fiber paper: (a) AFCM, (b) AFCSM.

3.5.2 Dielectric strength of AFCSM

Figure 10b presents the dielectric strength of AFCSM composites. The base composite (0% mica) exhibited a dielectric strength of 3.37 kV/mm, identical to that of AFCM, confirming that silicone resin alone does not significantly affect the insulation performance of the fiber network [15]. With increasing mica content, the dielectric strength of AFCSM followed a trend similar to that of AFCM, but with notably higher values at mica contents ≥30%. At 40% mica, AFCSM achieved a dielectric strength of 12.02 kV/mm, representing a 19% improvement over the 10.14 kV/mm of AFCM-40 [16].

This additional enhancement at high mica loadings is attributed to the synergistic effect of silicone resin and the surfactant AEO on mica dispersion. AEO promotes uniform distribution of mica flakes throughout the fiber network, minimizing agglomeration and ensuring that the flakes effectively bridge gaps between fibers [18]. Silicone resin then forms strong interfacial bonds with both fibers and mica, creating a cohesive "mica-resin-fiber" ternary insulation system [15]. This integrated structure further densifies the network and reduces the presence of micro-voids that could serve as breakdown initiation sites [19]. The resin also likely contributes to a more uniform electric field distribution by smoothing local field enhancements at fiber-mica interfaces, although further investigation is needed to confirm this mechanism [17].

3.6 Hydrophobic properties of composite papers

Surface hydrophobicity is essential for insulating materials used in humid environments, as water absorption can degrade both mechanical and electrical performance. The composite papers were treated with a hydrophobic sizing agent (TF-3002R), and their water repellency was evaluated by static water contact angle measurements.

Figure 11a illustrates the hydrophobic treatment process. After sizing, the papers were dried at 105 °C for 6 h to ensure complete curing of the hydrophobic layer. Figure 11b schematically depicts the working principle: the hydrophobic agent forms a low-surface-energy coating on the fiber and mica surfaces, shielding hydrophilic sites and preventing water molecule adsorption [16]. Figure 11c presents the contact angle results for AFCM and AFCSM before and after hydrophobic treatment. Untreated AFCM exhibited a contact angle of 48.5°, indicating hydrophilic behavior. Untreated AFCSM showed a slightly higher contact angle of 58°, attributable to the presence of silicone resin which reduces surface porosity and increases structural density, thereby limiting water penetration [15].

After hydrophobic treatment, the contact angles increased significantly to 102° for AFCM and 109° for AFCSM, both exceeding 100° and confirming successful conversion to hydrophobic surfaces [16]. The slightly higher value for AFCSM may reflect a more uniform coating due to the resin-modified surface chemistry [15].

These results demonstrate that the applied surface treatment effectively imparts hydrophobicity to the composite papers, which is critical for maintaining insulation reliability under humid conditions.

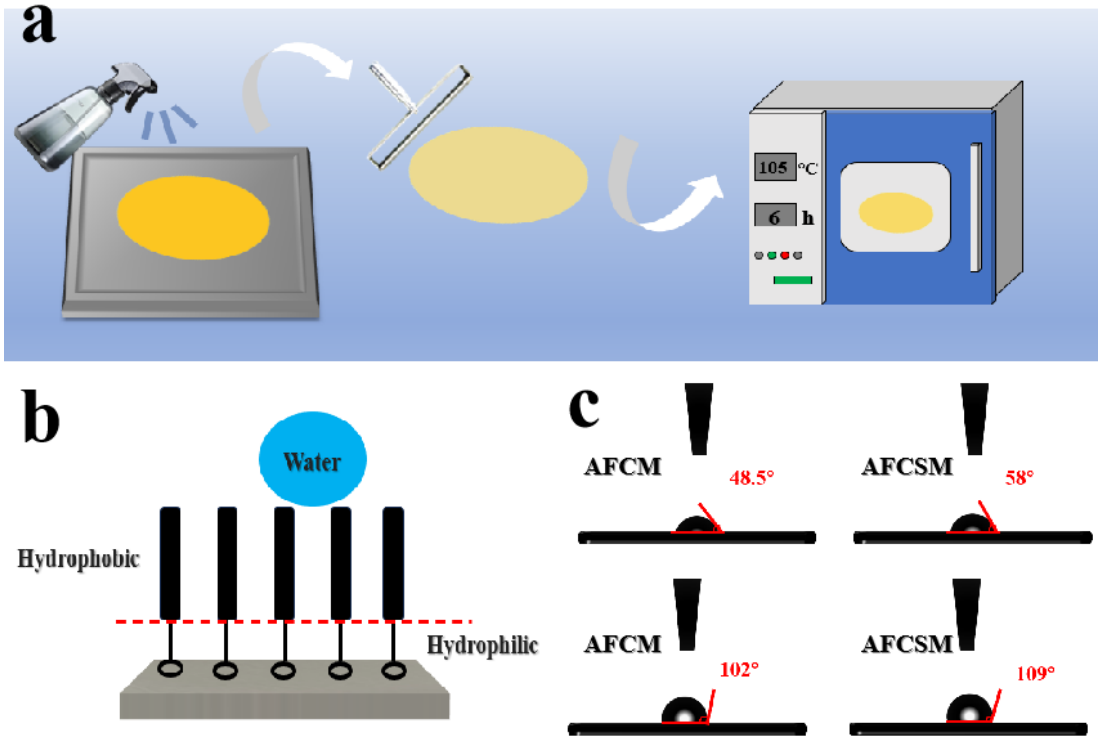

Figure 10. (a)Experiment on Hydrophobicity Improvement of Composite Fiber Paper. (b) hydrophobic principle. (c)Hydrophobic angle test of AFCM/AFCSM.

3.7 Thermal stability of composite paper

The thermal stability of the composite papers was evaluated by thermogravimetry (TG). Figure 12 A/B shows the TG and DTG curves for pure aluminum silicate fiber (AO) and three composite formulations: AFC (AO/CFS/AFS without resin), AFCS (AFC with silicone resin), and AFCSM (AFCS with 30% mica).

The AO sample exhibited a flat TG curve with no distinct endothermic or exothermic peaks throughout the tested temperature range (30–600 °C), indicating its excellent thermal stability and the absence of decomposition events below 600 °C [22]. AFCSM exhibits a gradual mass loss onset at 300 °C, attains thermal stability at 600 °C, and retains approximately 82% of its initial mass. AFCS initiates mass loss at the same temperature (300 °C) but displays a slightly higher mass loss rate compared with AFCSM; thermal stability is achieved at 650 °C, with a residual mass of 72%. AFC undergoes rapid mass loss beginning at 300 °C, with the most intense decomposition occurring between 500 °C and 600 °C; mass loss ceases completely at 650 °C, leaving a final residue of 66%.In contrast, all samples containing cellulose fibers (AFC, AFCS, AFCSM)

showed broad endothermic peaks between 500 and 600 °C, centered at approximately 550 °C. These peaks correspond to the thermal decomposition of cellulose, including depolymerization, dehydration, and char formation [23].

Among the composite samples, AFC displayed the most intense endothermic peak, indicating rapid heat absorption and vigorous decomposition of the cellulose component. The addition of silicone resin (AFCS) reduced the peak intensity, suggesting that the resin moderates the decomposition process, likely by forming a protective layer that delays heat transfer and mass loss [24,25]. The AFCSM composite, containing both silicone resin and mica, exhibited the broadest and lowest-magnitude endothermic peak. This indicates that mica further suppresses the heat absorption rate and enhances the overall thermal stability of the composite. The lamellar structure of mica acts as a physical barrier that hinders heat penetration and volatile release, while its inherent thermal stability contributes to the composite's resistance to high-temperature degradation [26].

These results demonstrate that the combination of silicone resin and mica synergistically improves the thermal stability of the aluminum silicate fiber-based composite paper, making it more suitable for applications requiring resistance to elevated temperatures.

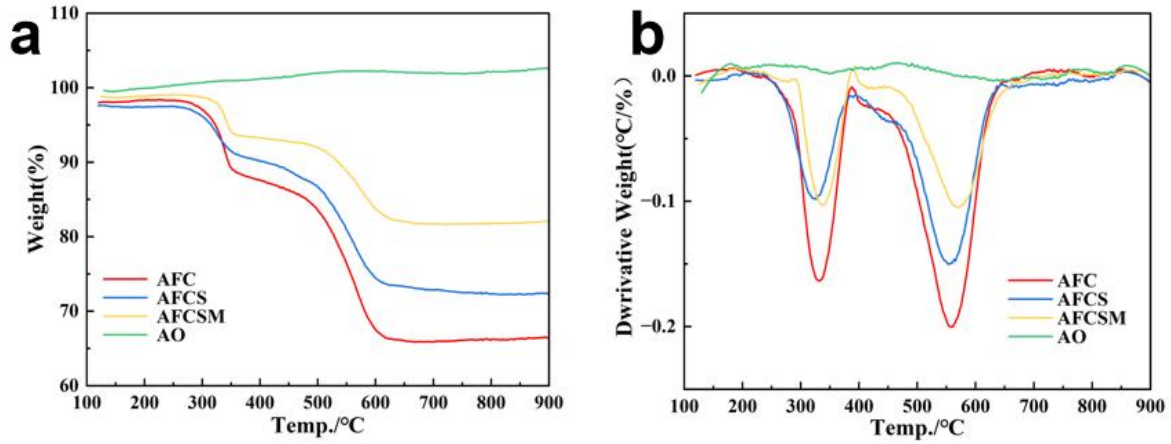

Figure 11.(a) TG curves of AO, AFC, AFCS, and AFCSM composite papers.(b)DTG curves of AO, AFC, AFCS, and AFCSM composite papers.

IV.CONCLUSION

This work demonstrates a feasible strategy for fabricating high-performance aluminum silicate fiber composite mica paper (AFCSM) via conventional filtration molding. By systematically varying the mica content (10–40 wt%) and comparing resin-containing (AFCSM) and resin-free (AFCM) formulations, we clarified the distinct roles of each component in determining the overall material performance. The addition of silicone resin (SI) significantly enhanced mechanical properties, increasing the optimal tensile strength from 1.35 MPa (AFCM at 10% mica) to 1.75 MPa (AFCSM at 20% mica). This improvement is attributed to the resin's ability to wet mica surfaces, reduce particle agglomeration, and promote stronger interfacial bonding between fibers and mica flakes [15].Mica content emerged as the primary factor controlling electrical insulation performance. Dielectric strength increased steadily with mica loading, reaching 12.02 kV/mm at 40% mica in the AFCSM composite—a 19% improvement over the resin-free counterpart. This enhancement results from the formation of a "mica-resin-fiber" ternary insulation system that effectively blocks conductive pathways [16,19]. Surface modification with hydrophobic agent TF-3002R successfully transformed the inherently hydrophilic composite papers into water-repellent materials, with contact angles exceeding 100° for both AFCM and AFCSM [16]. Thermal analysis showed that the combination of SI and mica progressively suppressed thermal decomposition, with AFCSM exhibiting the most stable thermal behavior among all tested formulations [25,26]. The AFCSM composite paper developed in this work achieves a balanced combination of mechanical strength (tensile strength >1.7 MPa), electrical insulation (dielectric strength >12 kV/mm), and hydrophobicity (contact angle >100°). These properties, together with the low-cost and scalable fabrication process, position this material as a promising candidate for electrical insulation applications in power batteries and other demanding environments where thermal management and electrical safety are critical. Future work will focus on optimizing the fiber-resin-mica interface and evaluating long-term performance under realistic operating conditions.

REFERENCES

[1]. Wang, L.; Yang, X.; Wang, Q.; Tian, H. Research on thermal out of control of lithium battery in new energy vehicles. IOP Conference Series: Earth and Environmental Science 2020, *446*(2), 022038.

[2]. Xu, Y.; Wang, Y.; Chen, D. Soot formation and its hazards in battery thermal runaway. Journal of Aerosol Science 2024, *181*, 106420.

[3]. Quan, T.; Xia, Q.; Wei, X.; Zhu, Y. Recent development of thermal insulating materials for Li-ion batteries. Energies 2024, *17*(17), 4412.

[4]. Liu, F.; Wang, J.; Yang, N.; Wang, F.; Chen, Y.; Lu, D.; et al. Experimental study on the alleviation of thermal runaway propagation from an overcharged lithium-ion battery module using different thermal insulation layers. Energy 2022, *257*, 124768.

[5]. Feng, J.; Ma, Z.; Wu, J.; Zhou, Z.; Liu, Z.; Hou, B.; et al. Fire-safe aerogels and foams for thermal insulation: from materials to properties. Advanced Materials 2025, *37*(3), 2411856.

[6]. Wang, Z.-Y.; Zhu, Y.-J.; Chen, Y.-Q.; Yu, H.-P.; Xiong, Z.-C. Flexible nanocomposite paper with superior fire retardance, mechanical properties and electrical insulation by engineering ultralong hydroxyapatite nanowires and aramid nanofibers. Chemical Engineering Journal 2022, *444*, 136470.

[7]. Hu, Y.; Zuo, Q.; Li, H.; Lei, L.; Xie, C.; Li, H. Fluorine-containing meta-aramid modified low dielectric, hydrophobic aramid paper. Composites Science and Technology 2025, *274*, 111444.

[8]. Yao, Y.; Zeng, X.; Sun, R.; Xu, J.-B.; Wong, C.-P. Highly thermally conductive composite papers prepared based on the thought of bioinspired engineering. ACS Applied Materials & Interfaces 2016, *8*(24), 15645-15653.

[9]. Zhang, H.; Zhang, M.; Li, J.; Yang, B.; Abbas, S.C.; Fu, C.; et al. Aramid nanofiber-based functional composite materials: Preparations, applications and perspectives. Composites Part B: Engineering 2024, *271*, 111151.

[10]. Tang, C.; Zhang, S.; Wang, X.; Hao, J. Enhanced mechanical properties and thermal stability of cellulose insulation paper achieved by doping with melamine-grafted nano-SiO_2. Cellulose 2018, *25*(6), 3619-3633.

[11]. Cheng, Z.; Gao, H.; Dai, H.; Zhang, H.; Yang, X.; Dong, X.; et al. Aluminosilicate Fiber-Reinforced Kaolinite Based Porous Materials: Dual Enhancement of Thermal Insulation and Mechanical Performance. Materials Chemistry and Physics 2025, *347*, 131421.

[12]. Pan, X.; Bao, Z.; Xu, W.; Gao, H.; Wu, B.; Zhu, Y.; et al. Recyclable nacre-like aramid-mica nanopapers with enhanced mechanical and electrical insulating properties. Advanced Functional Materials 2023, *33*(9), 2210901.

[13]. Parameswaranpillai, J.; Gopi, J.A.; Radoor, S.; D., M.D.C.; Krishnasamy, S.; Deshmukh, K.; et al. Turning waste plant fibers into advanced plant fiber reinforced polymer composites: A comprehensive review. Composites Part C: Open Access 2023, *10*, 100333.

[14]. Bastida, G.A.; Aguado, R.J.; Galván, M.V.; Zanuttini, M.Á.; Delgado-Aguilar, M.; Tarrés, Q. Impact of cellulose nanofibers on cellulose acetate membrane performance. Cellulose 2024, *31*(4), 2221-2238.

[15]. Ling, Y.; Qiu, B.; Wang, L.; Zhang, H.; Yang, Y.; Zhang, X.; et al. Phase morphology modulation of silicone-modified epoxy resins and effects on thermal, mechanical and ablative properties. Progress in Organic Coatings 2024, *196*, 108689.

[16]. Xu, K.; Wu, C.; Chen, Z.; Li, M.; Yang, L.; Ai, S.; Cui, S. Preparation and Characterization of Lightweight, Hydrophobic, and Insulative Melamine Foam/Fumed Silica Composites. ACS Applied Materials & Interfaces 2025, *17*(8), 12653-12662.

[17]. Zhou, C.; Cao, Y.; Chang, T.; Xia, G.; Li, Y.; Pan, T.; et al. Multilayer mica tailings-based aramid nanofiber composite films: A stable structural material with excellent mechanical and insulation properties. Materials Today Communications 2025, *46*, 112731.

[18]. Jiang, H.; Jiang, L.; Zhang, P.; Zhang, X.; Ma, N.; Wei, H. Force-induced self-assembly of supramolecular modified mica nanosheets for ductile and heat-resistant mica papers. Langmuir 2021, *37*(17), 5131-5138.

[19]. Zhao, Y.; Dang, W.; Si, L.; Lu, Z. Enhanced mechanical and dielectric properties of Aramid fiber/Mica-nanofibrillated cellulose composite paper with biomimetic multilayered structure. Cellulose 2019, *26*(3), 2035-2046.

[20]. Zhang, Z.; Feng, Y.; Wang, D.; Liang, L.; Wang, Z.; Yang, K.; et al. Thermal conductive network construction and enhanced thermal conductivity in mica tape composites for large generator insulation. Composites Science and Technology 2024, *254*, 110671.

[21]. Ashitha, P.N.; Shanker, T.B.; Parameshwaran, M.K.; Agarwal, S.; Gobinath, G.; Safvan, K.M.; Varughese, K.T. Nano Mica/Silicone Coating on Electrical Porcelain Substrate. IEEE Transactions on Dielectrics and Electrical Insulation 2023, *31*(2), 809-816.

[22]. Yu, L.; Zhou, S.; Zou, H.; Liang, M. Thermal stability and ablation properties study of aluminum silicate ceramic fiber and acicular wollastonite filled silicone rubber composite. Journal of Applied Polymer Science 2013, *131*(1).

[23]. Zárate, C.N.; Aranguren, M.I.; Reboredo, M.M. Thermal degradation of a phenolic resin, vegetable fibers, and derived composites. Journal of Applied Polymer Science 2008, *107*(5), 2977-2985.

[24]. Bo, J.; Zhang, K.; Cai, Q.; Zeng, T.; Zhu, M. Effect of homologous nano-composites on the thermal degradation of the silicone resin. Soft Materials 2016, *14*(4), 288-296.

[25]. Yang, Z.; Feng, L.; Diao, S.; Feng, S.; Zhang, C. Study on the synthesis and thermal degradation of silicone resin containing silphenylene units. Thermochimica Acta 2011, *521*(1-2), 170-175.

[26]. Saltas, V.; Pentari, D.; Vallianatos, F. Complex electrical conductivity of biotite and muscovite micas at elevated temperatures: A comparative study. Materials 2020, *13*(16), 3513.

[27]. Ji, D.; Zhang, M.; Sun, H.; Lyu, Y.; Cormier, S.L.; Ma, C.; et al. Nacre-inspired composite papers with enhanced mechanical and electrical insulating properties: Assembly of aramid papers with aramid nanofibers and basalt nanosheets. Journal of Materials Science & Technology 2025, *215*, 283-295.

[28]. Chen, X.; Zhang, T.; Sun, P.; Yu, F.; Li, B.; Dun, L. Study on the performance and mechanism of modified mica for improving polypropylene composites. International Journal of Low-Carbon Technologies 2022, *17*, 176-184.

[29]. Tang, L.; Jiang, J.; Liu, Q.; Li, Q.; Hu, Q.; Liu, X. A bioinspired, robust mica/chitosan/PBO nanofiber paper with excellent dielectric insulation properties and high thermal conductivity. Ceramics International 2025, *51*(19), 29752-29761.

[30]. Wei, W.; Zhang, Y.; Chen, H.; Su, Z.; Lan, D.; Zha, J. Nano-BN and nano-cellulose synergistically enhanced the mechanical, thermal, and insulating properties of cellulose insulating paper. Composites Science and Technology 2024, *256*, 110748.